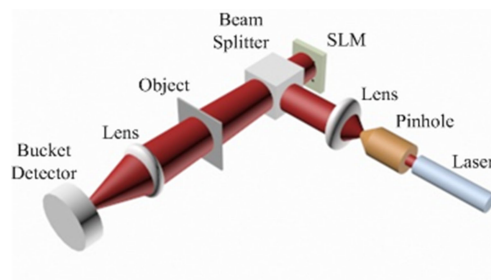


Fourier Spectrum Retrieval in Single-Pixel Imaging

Volume 11, Number 2, April 2019


Yin Xiao
Lina Zhou
Wen Chen



DOI: 10.1109/JPHOT.2019.2898658

1943-0655 © 2019 IEEE

Fourier Spectrum Retrieval in Single-Pixel Imaging

Yin Xiao,¹ Lina Zhou,¹ and Wen Chen ^{1,2}

¹Department of Electronic and Information Engineering, The Hong Kong Polytechnic University, Hong Kong, China

²The Hong Kong Polytechnic University Shenzhen Research Institute, Shenzhen 518057, China

DOI:10.1109/JPHOT.2019.2898658

1943-0655 © 2019 IEEE. Translations and content mining are permitted for academic research only.

Personal use is also permitted, but republication/redistribution requires IEEE permission.

See http://www.ieee.org/publications_standards/publications/rights/index.html for more information.

Manuscript received December 13, 2018; revised January 27, 2019; accepted February 7, 2019. Date of publication February 25, 2019; date of current version March 7, 2019. This work was supported by the National Natural Science Foundation of China under Grant 61605165 and in part by the Hong Kong Research Grants Council Early Career Scheme under Grant 25201416. Corresponding author: Wen Chen (e-mail: owen.chen@polyu.edu.hk).

Abstract: Fourier spectrum represents objects in the frequency domain. Low-frequency coefficients show outlines of objects, and high-frequency coefficients display details of objects. In this paper, we propose a novel and high-efficiency Fourier spectrum retrieval method in single-pixel imaging. First, a small percentage of low-frequency coefficients is measured based on the Fourier spectrum acquisition method. Then, high-frequency coefficients, which are not measured directly, are quickly and efficiently estimated by using the proposed method. In comparison with the conventional Fourier spectrum acquisition method, conventional correlation algorithm and conventional Gerchberg-Saxton-like algorithm, the proposed method shows great advantages in measurement efficiency, since the proposed method can obtain reconstructed objects with high signal-to-noise ratio by using far fewer measurements. In addition, the proposed method also shows its capability in reconstructing high-quality objects under noise contamination. The numerical results and discussion are presented to illustrate feasibility and effectiveness of the proposed method.

Index Terms: Fourier spectrum, single-pixel imaging, object reconstruction, optical imaging.

1. Introduction

Single-Pixel imaging (SPI) is an effective object reconstruction technique in recent years and has attracted more and more attention. Compared with a traditional two-dimensional (2D) charge-coupled device (CCD) which has a spatial resolution, a single-pixel detector (also called bucket detector) used in the SPI is a one-dimensional (1D) sensor and has no spatial resolution. The single-pixel detector has advantages of low cost and high signal-to-noise ratio (SNR). Under conditions of low light and especially non-visible light, the SPI shows obvious advantages over conventional imaging techniques with a CCD. The SPI emerges from ghost imaging (GI) which is also called correlation imaging [1]–[10]. The GI was first realized in quantum fields and considered as a quantum phenomenon. Subsequently, theories and experiments were conducted to realize GI in classical fields by using thermal light sources. In conventional GI, a laser beam passes through a rotating diffuser to generate pseudothermal light, and then the pseudothermal light is split into a signal beam and a reference beam. The signal beam interacts with an object, and the transmission light intensity is collected by a bucket detector. The reference beam is detected directly by a CCD. Object

reconstruction can be conducted by correlating the 1D signals detected by a bucket detector and the 2D speckle patterns detected by CCD. Computational GI (CGI) [5] further simplifies conventional GI setup by utilizing a spatial light modulator (SLM). When the SLM is used in GI, speckle patterns can be calculated directly, and then the reference beam path containing CCD in conventional GI can be removed. Since the quality of the reconstructed objects using GI is low, different techniques based on GI have been developed, such as differential GI (DGI) [11] and normalized GI (NGI) [12]. However, SNR values of the recovered objects by using these techniques have a linear relationship with respect to the number of measurements. It is further demonstrated that a Gerchberg-Saxton-like algorithm based on GI setup can improve the SNR [13]. This algorithm takes advantage of the integral property of Fourier transform and treats captured data as constraints for image reconstruction, which results in a nonlinear growth of the SNR value with respect to the number of measurements. Although improvements in SNR can be achieved by using the Gerchberg-Saxton-like algorithm, the algorithm still needs a large number of measurements, and the post-processing is time-consuming.

Compressive sensing (CS) achieves sub-Nyquist image acquisition by combining sampling and compression into a single linear measurement process [14]–[17], which has been applied in SPI. Since most objects are sparse in an appropriate basis (e.g., the discrete cosine transform basis), i.e., many zero coefficients after transformation, the CS is able to recover N -dimensional objects with M ($M < N$) measurements by using different kinds of optimization algorithms. Traditional object reconstruction techniques normally acquire object samples at or above the Nyquist rate (i.e., $M \geq N$), otherwise object reconstruction is an NP-hard problem. Hence, the CS methods have the capability to handle high-dimensional images or objects. However, under an optimization framework, the CS methods need large memory and a long time for computation, i.e., high computational complexity.

In contrast to the CS methods, Fourier spectrum acquisition method is an efficient and direct method to obtain Fourier spectrum coefficients in SPI. By designing illumination patterns in SPI, the Fourier spectrum coefficients can be calculated directly [18]–[27]. Since energy distribution of the objects concentrates on the central area of the Fourier spectrum, calculation of the coefficients located on the central area can achieve object reconstruction. Note that the CS methods estimate these coefficients through different optimization algorithms, and the Fourier spectrum acquisition method calculates them directly without computational complexity. Since the coefficients located on the central area, i.e., low-frequency coefficients, only denote outline of objects, high-frequency coefficients are needed to show details of objects. However, in conventional methods, to measure coefficients with all frequencies also means a large number of measurements, which is also time-consuming.

In this paper, we propose a novel method to recover high-SNR object with far fewer measurements in the SPI. When a small percentage of low-frequency coefficients are calculated based on the Fourier spectrum acquisition method, high-frequency coefficients can be estimated efficiently by using the proposed method and then high-SNR object reconstruction can be achieved. Compared with conventional Fourier spectrum acquisition method, conventional GI and conventional Gerchberg-Saxton-like algorithm, the proposed method shows a great advantage in measurement efficiency, since it uses far fewer measurements and has a fast convergence rate. In the case of noise contamination, the proposed method is still efficient and can also achieve high-SNR recovered objects.

2. Theoretical Analysis

A single-arm SPI setup is shown in Fig. 1.

As shown in Fig. 1, a monochromatic laser is expanded through a pinhole and then collimated by a lens. A beam splitter is used to illuminate the SLM. The SLM modulates the wave field and generates a sequence of speckle fields to illuminate an object. Then, the total light intensity transmitting through the object is sequentially collected by a bucket detector without spatial resolution. With the data captured by the detector and 2D speckle patterns stored in a computer, a correlation algorithm can

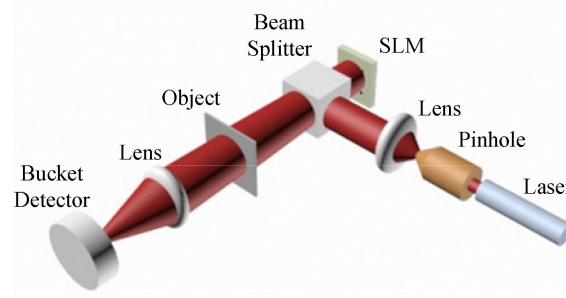


Fig. 1. Schematic of a single-arm SPI setup.

be used to reconstruct the object [6].

$$T_{GI}(x, y) = \frac{1}{M} \sum_{i=1}^M (B_i - \langle B_i \rangle) (P_i(x, y) - \langle P_i(x, y) \rangle), \quad (1)$$

where $\langle \bullet \rangle = \sum_i \bullet / M$ denotes an ensemble average over M measurements, P_i represents a pattern and B_i represents the corresponding single-pixel value detected by the bucket detector.

The SNR value of the reconstructed objects by using Eq. (1) has a linear relationship with respect to the number of measurements. In this case, to achieve a high-quality object reconstruction, a large number of measurements are necessary. Fourier spectrum acquisition method is an effective method to avoid a large number of measurements [18]. Since most objects are sparse in the Fourier domain, a small percentage of low-frequency Fourier spectrum coefficients are sufficient for object reconstruction. A definition of 2D discrete Fourier transform pair is shown in Eqs. (2) and (3).

$$G(p, q) = \sum_{m=-M/2}^{M/2-1} \sum_{n=-N/2}^{N/2-1} g(m, n) \exp \left[-j2\pi \left(\frac{pm}{M} + \frac{qn}{N} \right) \right], \quad (2)$$

$$g(m, n) = \frac{1}{MN} \sum_{p=-M/2}^{M/2-1} \sum_{q=-N/2}^{N/2-1} G(p, q) \exp \left[j2\pi \left(\frac{pm}{M} + \frac{qn}{N} \right) \right], \quad (3)$$

where $g(m, n)$ denotes an object, m and n denote coordinates of the object, M and N represent dimensions of the object, $G(p, q)$ denotes Fourier spectrum of the object, and p and q represents coordinates of the Fourier spectrum. Since the exponential part in Eq. (2) consists of complex numbers, it is not easy to realize such a form in real optical experiments. The patterns used in the Fourier spectrum acquisition method are sinusoidal forms, which can be expressed as

$$P_\psi = a + b \cos \left(2\pi \frac{p}{M} m + 2\pi \frac{q}{N} n + \psi \right), \quad (4)$$

where a is a constant equal to the average intensity of the object, b is a scale factor which is also a constant, and ψ is the phase which normally has four values, i.e., 0 , $\pi/2$, π and $3\pi/2$. Hence, a 4-step Fourier spectrum acquisition method can be expressed as

$$B_0 = \sum_m \sum_n g(m, n) P_0 = \sum_m \sum_n g(m, n) \left[a + b \cos \left(2\pi \frac{p}{M} m + 2\pi \frac{q}{N} n \right) \right] \quad (5)$$

$$B_{\pi/2} = \sum_m \sum_n g(m, n) P_{\pi/2} = \sum_m \sum_n g(m, n) \left[a - b \sin \left(2\pi \frac{p}{M} m + 2\pi \frac{q}{N} n \right) \right], \quad (6)$$

$$B_\pi = \sum_m \sum_n g(m, n) P_\pi = \sum_m \sum_n g(m, n) \left[a - b \cos \left(2\pi \frac{p}{M} m + 2\pi \frac{q}{N} n \right) \right], \quad (7)$$

$$B_{3\pi/2} = \sum_m \sum_n g(m, n) P_{3\pi/2} = \sum_m \sum_n g(m, n) \left[a + b \sin \left(2\pi \frac{p}{M} m + 2\pi \frac{q}{N} n \right) \right], \quad (8)$$

where B_0 , $B_{\pi/2}$, B_π and $B_{3\pi/2}$ are four single-pixel values corresponding to four different phases. With these four values, each coefficient can be constructed by

$$\begin{aligned}
 & (B_0 - B_\pi) + j(B_{\pi/2} - B_{3\pi/2}) \\
 &= 2b \left[\sum_m \sum_n g(m, n) \cos\left(2\pi \frac{p}{M}m + 2\pi \frac{q}{N}n\right) - j \sum_m \sum_n g(m, n) \sin\left(2\pi \frac{p}{M}m + 2\pi \frac{q}{N}n\right) \right] \\
 &= 2b \sum_m \sum_n g(m, n) \exp\left[-j2\pi \left(\frac{p}{M}m + \frac{q}{N}n\right)\right] \\
 &= 2bG(p, q),
 \end{aligned} \tag{9}$$

and then we get

$$G(p, q) = \frac{1}{2b} [(B_0 - B_\pi) + j(B_{\pi/2} - B_{3\pi/2})]. \tag{10}$$

When all coefficients or a part of coefficients are calculated, object reconstruction can be further carried out in Eq. (3). Since low-frequency coefficients denote outlines of the objects and high-frequency coefficients represent details of the objects, it is necessary to measure coefficients from low frequency to high-frequency in order to achieve high-quality reconstructed objects. Hence, in this case, the measurement efficiency is not high. Here, a high-efficiency Fourier spectrum retrieval method is proposed. In contrast to the measurement of all the Fourier spectrum coefficients in SPI, the proposed method can achieve high-SNR object reconstruction using only a small part of low-frequency Fourier spectrum coefficients. High-frequency spectrum coefficients can be estimated efficiently by using the proposed method. Before introducing the proposed method, an important property in SPI is introduced firstly. A single-pixel detection process can be given by

$$B = \sum_m \sum_n g(m, n) P(m, n). \tag{11}$$

A Fourier transform property corresponding to this process, i.e., Eq. (11), is described by

$$F\{g(m, n) \odot P(m, n)\}_{k=0} = B \tag{12}$$

where F represents Fourier transform, \odot denotes element-wise production between two matrices and $k = 0$ denotes zero-frequency component. To better understand the meaning of Eq. (12), Fig. 2 shows a schematic to illustrate the relationship.

As shown in Fig. 2, a picture with sinusoidal values is used to represent a pattern P , and a USAF 1951 target picture is used to represent the object g . The grid picture in Fig. 2 represents the Fourier spectrum of $g \odot P$, and the central value (i.e., zero-frequency component) in the Fourier spectrum is equal to the value detected by the bucket detector in SPI. Hence, such a property can be utilized to make the captured data as constraints in the proposed method. In addition, the calculated low-frequency spectrum coefficients can also act as constraints in the proposed method, which can lead to a fast convergence rate. With these two constraints, high-frequency coefficients can be calculated efficiently when only a small part of low-frequency Fourier spectrum coefficients are used in the proposed method. A process of the proposed method is shown as follows:

- 1) Utilize the Fourier spectrum acquisition method to calculate a small part of low-frequency spectrum coefficients, and then reconstruct an initial guess T .
- 2) Multiply the initial guess T with a pattern P to generate a target object I_{tar} ,

$$I_{tar} = P \odot T. \tag{13}$$

- 3) Do Fourier transform (FT) for the target object to get its spectrum $F(I_{tar})$.
- 4) Utilize the single-pixel value B detected by bucket detector in SPI to replace the zero-frequency component in spectrum $F(I_{tar})$, and get a new spectrum $F'(I_{tar})$.
- 5) Do inverse Fourier transform (IFT) for $F'(I_{tar})$ to get an updated target object I'_{tar} .

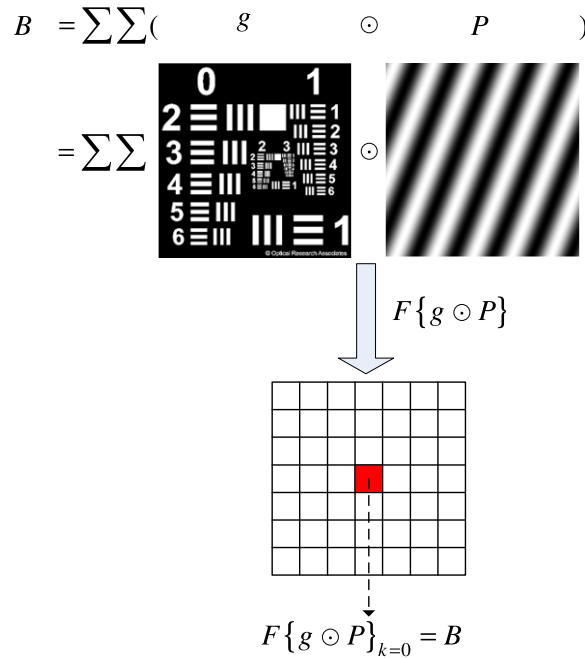


Fig. 2. Schematic to show the relationship between Eqs. (11) and (12).

6) Update the initial guess T by

$$T' = T + \frac{P}{\max(P^2 + \alpha)} \odot (I'_{tar} - I_{tar}) \quad (14)$$

where α is a small constant used to make denominator non-zero, and max is used to get a maximum.

- 7) Do FT of T' to get its spectrum $F(T')$.
- 8) Utilize the small part of low-frequency spectrum coefficients to replace the corresponding coefficients in $F(T')$, and then get a new spectrum $F'(T')$.
- 9) Do IFT for $F'(T')$ to generate a new initial guess T_{new} .
- 10) Repeat steps (2)-(9) for all measurements until a certain criterion is satisfied. The criterion is defined as the square error between T at the n th iteration and T_{new} obtained at the $(n + 1)$ th iteration, and a threshold is set to break the iterative process. Here, when all measurements are used, one iteration is completed.

A flow chart of the proposed method is further shown in Fig. 3.

The right part in Fig. 3 can be considered as an extension of conventional Gerchberg-Saxton-like algorithm. In conventional Gerchberg-Saxton-like algorithm, there is only one constraint (i.e., the single-pixel value) in spatial domain. Here, the calculated low-frequency coefficients provide another constraint in Fourier domain, which can enhance convergence of the proposed algorithm. By using the known data (i.e., single-pixel value and the calculated low-frequency coefficients) as shown in Fig. 3, the unknown high-frequency coefficients could be estimated progressively using a series of iterations. The principles in the proposed method are established by using phase retrieval concept [28], [29], which can effectively resolve the object reconstruction problem in the SPI [18]–[27], [30].

3. Results and Discussion

In this study, the ratio of Fourier spectrum coefficients is defined as

$$\text{Ratio} = \frac{\text{Number of coefficients measured}}{\text{Number of total pixels}}. \quad (15)$$

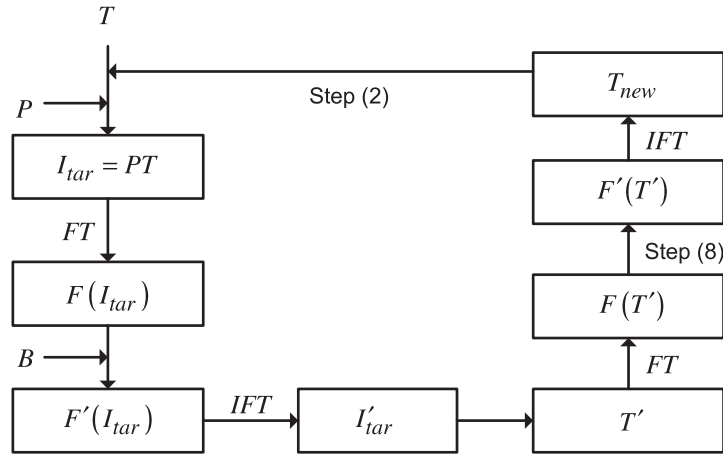


Fig. 3. Flow chart of the proposed method.

Fig. 4. (a) Reconstructed object (64×64 pixels) using 10% Fourier spectrum coefficients, (b) reconstructed object (64×64 pixels) by using the proposed method, and (c) reconstructed object (64×64 pixels) using 90% Fourier spectrum coefficients.

Table 1
Parameters of the Reconstructed Objects in Figs. 4(a)–4(c)

	The number of measurements	SNR
Fig. 4(a)	924	1.80
Fig. 4(b)	924	63.34
Fig. 4(c)	7564	46.13

To quantitatively evaluate quality of the reconstructed objects, SNR is used to estimate the difference between reconstructed objects and original objects, which is defined as [31]

$$\text{SNR} = \frac{\sum \sum (g - \bar{g})^2}{\sum \sum (T - g)^2}, \quad (16)$$

where \bar{g} denotes the mean value of g .

As shown in Fig. 4(a), a reconstructed object using only 10% Fourier spectrum coefficients has low contrast, because high-frequency components which contain details of the objects are lost. However, when the reconstructed object in Fig. 4(a) is taken as an initial guess in our proposed method, the lost high-frequency components can be estimated efficiently, and a high-SNR reconstructed object can be recovered, as shown in Fig. 4(b). For comparison, a reconstructed object using direct measurement of 90% Fourier spectrum coefficients is further shown in Fig. 4(c). Although most high-frequency components are calculated directly in Fig. 4(c), the reconstructed object in Fig. 4(b) still has a higher SNR than that in Fig. 4(c). Detailed parameters of the recovered objects in Figs. 4(a)–4(c) are shown in Table 1.

As shown in Table 1, the number of measurements used for reconstructing the object in Fig. 4(a) is 924, and the corresponding SNR value is low, i.e., 1.80. This is due to the measurement of only

Table 2
Improvement of the SNR in Different Sampling Ratios

Ratio	The number of measurements	k	SNR 1	SNR 2
2%	264	46	0.79	3.54
4%	364	48	1.22	5.28
6%	612	30	1.29	19.53
8%	760	17	1.68	54.87
10%	924	9	1.80	64.34
12%	1104	5	2.25	70.17

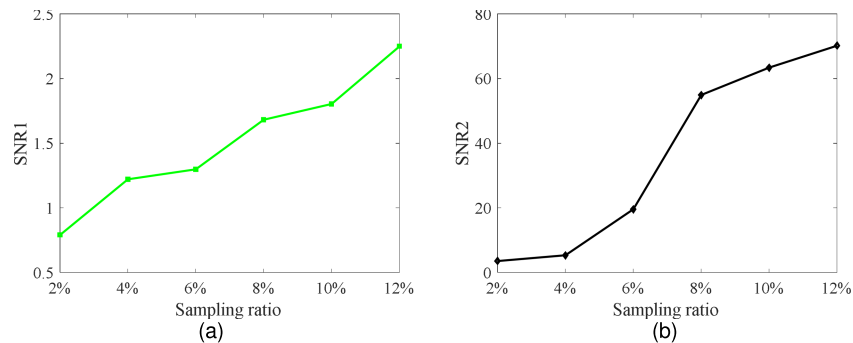


Fig. 5. (a) SNR1 versus sampling measurement ratio, and (b) SNR2 versus sampling measurement ratio. SNR1 represents SNR values of the reconstructed objects using conventional Fourier spectrum acquisition method, and SNR2 represents SNR values of the reconstructed objects using the proposed method.

a small part of low-frequency components. However, it can be seen in Table 1, without additional measurements, the proposed method can increase the SNR to a large value, i.e., 63.34, which means that high-frequency components are estimated efficiently. The number of measurements used to recover the object in Fig. 4(c) is 7564 which realizes the measurement of 90% Fourier spectrum coefficients, and SNR of the reconstructed object is 46.13. Hence, when high-frequency components are measured, SNR can have a dramatic enhancement. In the proposed method, although high-frequency components are not measured directly, they can be obtained efficiently by using the proposed method, which is verified in Fig. 4(b).

In order to investigate performance of the proposed method in different measurement ratios, the ratios of Fourier spectrum coefficients ranging from 2% to 12% are tested, and the corresponding results are given in Table 2.

In Table 2, SNR1 represents SNR values of the reconstructed objects by using conventional Fourier spectrum acquisition method, and SNR2 represents SNR values of the reconstructed objects by using the proposed method. k denotes the number of iterations used in the proposed method. As shown in Table 2, SNR1 increases slowly as the ratio increases. However, SNR2 has a dramatic enhancement with respect to measurement ratio. In addition, as the measurement ratio increases, the number of iterations used in the proposed method decreases quickly, which means that the method has a fast convergence rate. As the number of measurements increases, quality of the initial guess becomes better, which means that more useful information (i.e., more constraints) is offered to the proposed method and the convergence rate of the proposed method becomes faster, which can also be seen in Table 2. For a given ratio, it is worth noting that the number of measurements represents the total amount of patterns used in the 4-step Fourier spectrum acquisition method.

In Fig. 5(a), it is clear that in conventional method, quality of reconstructed objects becomes better as the sampling measurement ratio increases. However, the SNR has a slow rate to increase, since it ranges from 0.79 to 2.25 in the given different sampling ratios. However, it is obvious that there

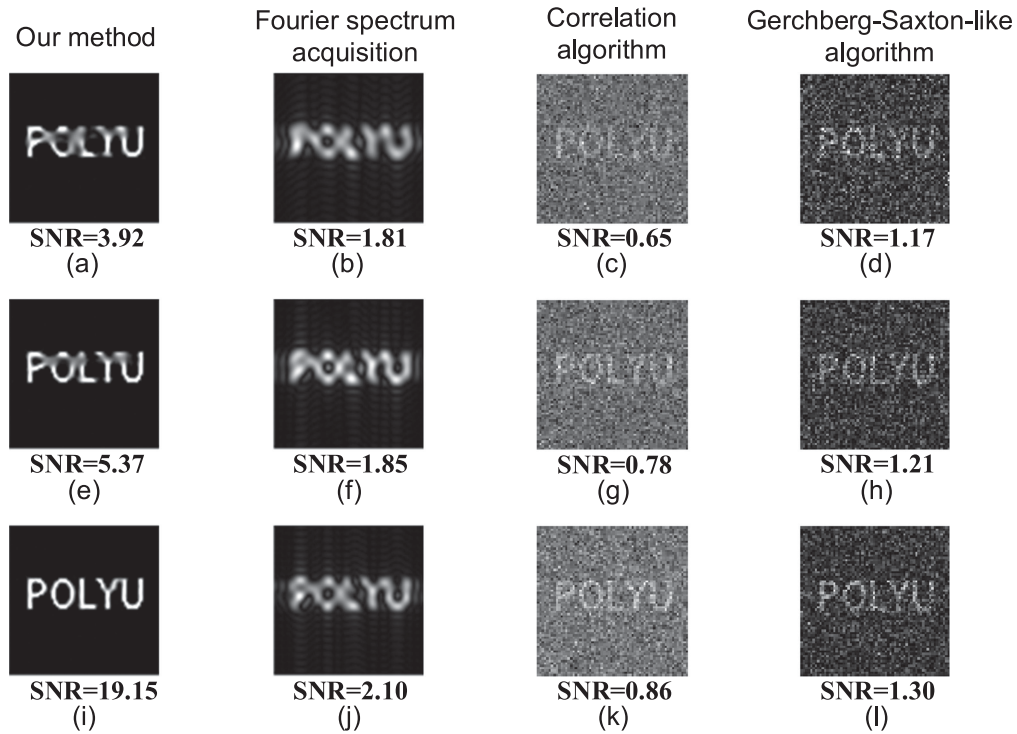


Fig. 6. Comparisons of reconstructed objects (64×64 pixels) by using the proposed method and conventional methods. (a), (e) and (i) reconstructed objects by using the proposed method, (b), (f) and (j) reconstructed objects by using Fourier spectrum acquisition method, (c), (g) and (k) reconstructed objects by using correlating algorithm, (d), (h) and (l) reconstructed objects by using Gerchberg-Saxton-like algorithm; in the first row, the number of measurements is 612; in the second row, the number of measurements is 760; in the third row, the number of measurements is 924.

is a dramatic enhancement in SNR2 values when the proposed method is utilized. As shown in Fig. 5(b), in the given different sampling ratios, the SNR values are from 3.54 to 70.18, which is a bigger region than that in Fig. 5(a).

To further illustrate advantages of the proposed method, a comparison among the proposed method, conventional Fourier spectrum acquisition method, conventional GI (i.e., correlation algorithm), and conventional Gerchberg-Saxton-like algorithm is conducted, which is illustrated in Fig. 6.

As shown in Fig. 6, with the same number of measurements, the proposed method has a better performance than conventional methods. Results in Figs. 6(b), (f) and (j) are obtained by using conventional Fourier spectrum acquisition method when only a small part of coefficients (i.e., low-frequency part) are measured. It can be seen that the reconstructed objects show rough outlines. The lost high-frequency part can be further estimated by using the proposed method. When more low-frequency coefficients are measured, high-frequency coefficients can be estimated more exactly which is demonstrated in Figs. 6(a), (e) and (i). For conventional GI (i.e., correlation algorithm), object reconstruction is a result of statistic average, and object reconstruction needs a large number of measurements which are normally larger than the total number of pixels of the object. For an object with size 64×64 , the total pixel number is 4096. Hence, when the number of measurements is less than 4096, quality of reconstructed objects by using conventional correlation algorithm is low, as shown in Figs. 6(c), (g) and (k). As introduced in Section I, conventional Gerchberg-Saxton-like algorithm is an effective method to improve quality of reconstructed objects, and the SNR values can have a nonlinear growth with respect to the number of measurements. However, such a method

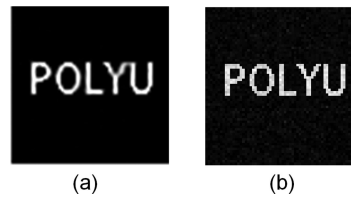


Fig. 7. (a) Reconstructed object (64×64 pixels) by using the proposed method, and (b) reconstructed object (64×64 pixels) by using conventional Gerchberg-Saxton-like algorithm.

Table 3
Parameters Used for the Proposed Method and Conventional Gerchberg-Saxton-Like Algorithm

	SNR	The number of measurements	Iterations	Threshold	Time
Our method	19.15	924	9	10^{-4}	4.4s
Gerchberg-Saxton-like algorithm	18.34	4000	1164	10^{-10}	1441.6s

still needs a large number of measurements, otherwise it cannot obtain the desired results as shown in Figs. 6(d), (h) and (l).

A further comparison between the proposed method and conventional Gerchberg-Saxton-like algorithm at the same SNR level is shown in Fig. 7.

In Fig. 7, reconstructed objects respectively obtained by using the proposed method and conventional Gerchberg-Saxton-like algorithm have a small difference in SNR values (i.e., 19.15 and 18.34). However, parameters used to recover them have a great difference, which is shown in Table 3. The number of measurements used in the proposed method is 924, while it is 4000 to be used in conventional Gerchberg-Saxton-like algorithm. The number of iterations used in the proposed method is only 9, which is far fewer than that used in conventional Gerchberg-Saxton-like algorithm, i.e., 1164. In addition, the thresholds acting as convergence criteria are also different between two methods. Compared with 10^{-4} used in the proposed method, 10^{-10} is a much stricter criterion in conventional method, and therefore is not easy to approach, which is also demonstrated from the computational time, as shown in Table 3.

Grayscale objects are also tested by using the proposed method. Compared with grayscale objects, binary objects can be more effectively recovered by using the proposed method. It is also found that for recovering large-size (e.g., 256×256 pixels) or low-size objects, performance of the proposed method is similar.

To test performance of the proposed method at different noise levels, a definition of noise strength ρ used in this paper is given as

$$B = \sum_m \sum_n g(m, n) P(m, n) + \sum_m \sum_n \rho * R(m, n), \quad (17)$$

where $R(m, n)$ represents Gaussian noise with mean of 0 and variance of 1. It is worth noting that the object $g(m, n)$ and pattern $P(m, n)$ have pixel values ranging from 0 to 1.

The initial guesses used at different noise strengths (i.e., 0, 0.01, 0.03 and 0.05) are obtained by using the Fourier spectrum acquisition method with 924 measurements, which are respectively shown in Figs. 8(a), (b), (c) and (d). Although random noise is considered, the proposed method still shows its powerful capability in reconstructing high-SNR objects, as shown in Figs. 8(e), (f), (g) and (h). Detailed information of the reconstructed objects in Fig. 8 is further shown in Table 4 and Fig. 9. SNR1 represents SNR values of the reconstructed objects using conventional Fourier spectrum acquisition method, and SNR2 represents SNR values of the reconstructed objects using the proposed method.

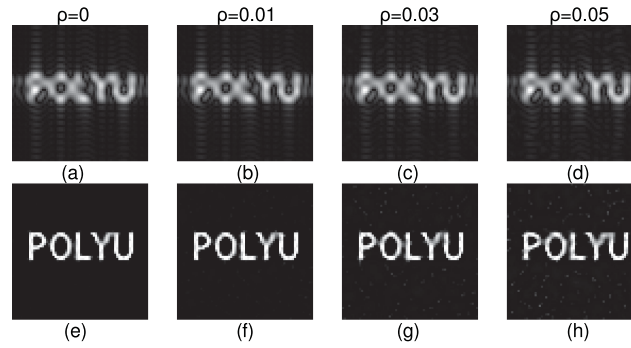


Fig. 8. (a), (b), (c) and (d) initial guess obtained by using Fourier spectrum acquisition method in different noisy conditions, and (e), (f), (g) and (h) recovered high-quality objects by using the proposed method in different noisy conditions.

Table 4
A comparison in Different Noisy Conditions by Using the Proposed Method

	$\rho=0$	$\rho=0.01$	$\rho=0.03$	$\rho=0.05$
SNR1	2.10	2.10	2.09	2.08
The number of iterations	9	6	2	1
SNR2	19.15	15.49	11.36	9.43

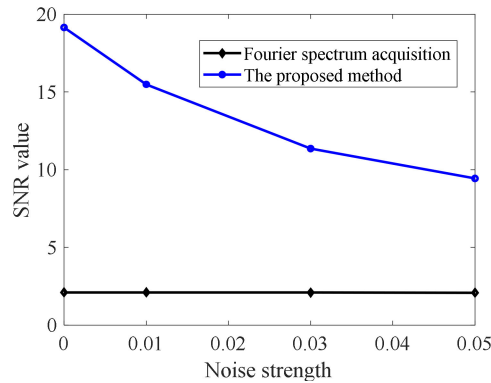


Fig. 9. SNR value versus noise strength by using conventional Fourier spectrum acquisition method and the proposed method.

It is clear that noise has an effect on object reconstructions, which can be seen from SNR2 values. However, the noise does not affect the fast convergence rate, since the number of iterations is still small. It is found that the proposed method is still suitable to recover high-SNR objects in SPI under noisy conditions. It is worth noting that similarly to other methods, large noise strengths could deteriorate quality of reconstructed objects, since large noise strengths have an effect on data accuracy, i.e., single-pixel values.

4. Conclusion

We have proposed a novel and efficient method to recover high-SNR objects in the SPI. A small part of low-frequency coefficients in Fourier spectrum is utilized to retrieve high-frequency components in the proposed method. The proposed method shows obvious advantages over conventional methods, e.g., Fourier spectrum acquisition method, correlation algorithm and the Gerchberg-Saxton-like algorithm. Compared with conventional methods, the proposed method achieves high-

SNR reconstructed objects with far fewer measurements as verified by numerical results, and has a fast convergence rate. In addition, the proposed method is also a powerful tool to recover high-SNR objects in noisy conditions.

References

- [1] T. B. Pittman, Y. H. Shih, D. V. Strekalov, and A. V. Sergienko, "Optical imaging by means of two-photon quantum entanglement," *Phys. Rev. A*, vol. 52, no. 5, pp. R3429–R3432, Nov. 1995.
- [2] D. V. Strekalov, A. V. Sergienko, D. N. Klyshko, and Y. H. Shih, "Observation of two-photon "ghost" interference and diffraction," *Phys. Rev. Lett.*, vol. 74, no. 18, May 1995, Art. no. 3600.
- [3] A. Gatti, E. Brambilla, M. Bache, and L. A. Lugiato, "Ghost imaging with thermal light: Comparing entanglement and classical correlation," *Phys. Rev. Lett.*, vol. 93, no. 9, Aug. 2004, Art. no. 093602.
- [4] A. Valencia, G. Scarcelli, M. D'Angelo, and Y. Shih, "Two-photon ghost imaging with thermal light," *Phys. Rev. Lett.*, vol. 94, no. 6, Feb. 2005, Art. no. 063601.
- [5] J. H. Shapiro, "Computational ghost imaging," *Phys. Rev. A*, vol. 78, no. 6, Dec. 2008, Art. no. 061802R.
- [6] Y. Bromberg, O. Katz, and Y. Silberberg, "Ghost imaging with a single detector," *Phys. Rev. A*, vol. 79, no. 5, May 2009, Art. no. 053840.
- [7] K. W. C. Chan, M. N. O'Sullivan, and R. W. Boyd, "High-order thermal ghost imaging," *Opt. Lett.*, vol. 34, no. 21, pp. 3343–3345, Nov. 2009.
- [8] B. I. Erkmen and J. H. Shapiro, "Ghost imaging: From quantum to classical to computational," *Adv. Opt. Photon.*, vol. 2, no. 4, pp. 405–450, Aug. 2010.
- [9] R. E. Meyers, K. S. Deacon, and Y. Shih, "Turbulence-free ghost imaging," *Appl. Phys. Lett.*, vol. 98, no. 11, Feb. 2011, Art. no. 111115.
- [10] W. Chen and X. D. Chen, "Marked ghost imaging," *Appl. Phys. Lett.*, vol. 104, no. 25, May 2014, Art. no. 251109.
- [11] F. Ferri, D. Magatti, L. A. Lugiato, and A. Gatti, "Differential ghost imaging," *Phys. Rev. Lett.*, vol. 104, no. 25, Jun. 2010, Art. no. 219902.
- [12] B. Q. Sun, S. S. Welsh, M. P. Edgar, J. H. Shapiro, and M. J. Padgett, "Normalized ghost imaging," *Opt. Express*, vol. 20, no. 15, pp. 16892–16901, Jul. 2012.
- [13] W. Wang, X. M. Hu, J. D. Liu, S. Z. Zhang, J. L. Suo, and G. H. Situ, "Gerchberg-Saxton-like ghost imaging," *Opt. Express*, vol. 23, no. 22, pp. 28416–28422, Nov. 2015.
- [14] D. L. Donoho, "Compressed sensing," *IEEE Trans. Inf. Theory*, vol. 52, no. 4, pp. 1289–1306, Apr. 2006.
- [15] E. J. Candes, J. Romberg, and T. Tao, "Robust uncertainty principles: Exact signal reconstruction from highly incomplete frequency information," *IEEE Trans. Inf. Theory*, vol. 52, no. 2, pp. 489–509, Feb. 2006.
- [16] M. F. Duarte *et al.*, "Single-pixel imaging via compressive sampling," *IEEE Signal Process. Mag.*, vol. 25, no. 2, pp. 83–91, Mar. 2008.
- [17] W. L. Chan, K. Charan, D. Takhar, K. F. Kelly, R. G. Baraniuk, and D. M. Mittleman, "A single-pixel terahertz imaging system based on compressed sensing," *Appl. Phys. Lett.*, vol. 93, no. 12, Sep. 2008, Art. no. 121105.
- [18] Z. Zhang, X. Ma, and J. Zhong, "Single-pixel imaging by means of Fourier spectrum acquisition," *Nature Comm.*, vol. 6, no. 6225, Feb. 2015.
- [19] L. Bian, J. Suo, X. Hu, F. Chen, and Q. Dai, "Efficient single pixel imaging in Fourier space," *J. Opt.*, vol. 18, no. 8, Jul. 2016, Art. no. 085704.
- [20] B. L. Liu, Z. H. Yang, X. Liu and L. A. Wu, "Coloured computational imaging with single-pixel detectors based on a 2D discrete cosine transform," *J. Mod. Opt.*, vol. 64, no. 3, pp. 259–264, Sep. 2016.
- [21] J. Huang, D. Shi, K. Yuan, S. X. Hu, and Y. J. Wang, "Computational-weighted Fourier single-pixel imaging via binary illumination," *Opt. Express*, vol. 26, no. 13, pp. 16475–16559, Jun. 2018.
- [22] H. Z. Jiang, S. G. Zhu, H. J. Zhao, B. J. Xu, and X. D. Li, "Adaptive regional single-pixel imaging based on the Fourier slice theorem," *Opt. Express*, vol. 25, no. 13, pp. 15118–15130, May 2017.
- [23] H. D. Ren, S. M. Zhao, and J. Gruska, "Edge detection based on single-pixel imaging," *Opt. Express*, vol. 26, no. 5, pp. 5501–5511, Feb. 2018.
- [24] B. J. Xu, H. Z. Jiang, H. J. Zhao, X. D. Li, and S. G. Zhu, "Projector-defocusing rectification for Fourier single-pixel imaging," *Opt. Express*, vol. 26, no. 4, pp. 5005–5017, Feb. 2018.
- [25] Z. B. Zhang, S. J. Liu, J. Z. Peng, M. H. Yao, G. A. Zheng, and J. G. Zhong, "Simultaneous spatial, spectral, and 3D compressive imaging via efficient Fourier single-pixel measurements," *Optica*, vol. 5, no. 3, pp. 315–319, Mar. 2018.
- [26] Z. B. Zhang, S. M. Jiao, M. H. Yao, X. Li, and J. G. Zhong, "Secured single-pixel broadcast imaging," *Opt. Express*, vol. 26, no. 11, pp. 14578–14591, May 2018.
- [27] Z. B. Zhang, X. Y. Wang, G. A. Zheng, and J. G. Zhong, "Fast Fourier single-pixel imaging via binary illumination," *Sci. Rep.*, vol. 7, Sep. 2017, Art. no. 12029.
- [28] J. R. Fienup, "Reconstruction of an object from the modulus of its Fourier transform," *Opt. Lett.*, vol. 3, no. 1, pp. 27–29, Jul. 1978.
- [29] J. R. Fienup, "Phase retrieval algorithms: A comparison," *Appl. Opt.*, vol. 21, no. 15, pp. 2758–2769, Aug. 1982.
- [30] K. M. Czajkowski, A. Pastuszczyk, and R. Kotyński, "Real-time single-pixel video imaging with Fourier domain regularization," *Opt. Express*, vol. 26, no. 16, pp. 20009–20022, Jul. 2018.
- [31] X. R. Yao, W. K. Yu, X. F. Liu, L. Z. Li, L. A. Wu, and G. J. Zhai, "Iterative denoising of ghost imaging," *Opt. Express*, vol. 22, no. 20, pp. 24268–24275, Oct. 2014.